NANO LETTERS

Letter

pubs.acs.org/NanoLett

Graphene Sublattice Symmetry and Isospin Determined by Circular Dichroism in Angle-Resolved Photoemission Spectroscopy

Isabella Gierz,*[,†,⊥] Matti Lindroos,[‡] Hartmut Höchst,[§] Christian R. Ast,[†] and Klaus Kern[†,∥]

[†]Max-Planck-Institut für Festkörperforschung, D-70569 Stuttgart, Germany

[‡]Department of Physics, Tampere University of Technology, 33101 Tampere, Finland

[§]Synchrotron Radiation Center, University of Wisconsin-Madison, Stoughton, Wisconsin 53589, United States

[∥]Institut de Physique de la Matière Condensée, Ecole Polytechnique Fédérale de Lausanne, CH-1015 Lausanne, Switzerland

Supporting Information

ABSTRACT: The Dirac-like electronic structure of graphene originates from the equivalence of the two basis atoms in the honeycomb lattice. We show that the characteristic parameters of the initial state wave function (sublattice symmetry and isospin) can be determined using angle-resolved photoemission spectroscopy (ARPES) with circularly polarized synchrotron radiation. At a photon energy of $h\nu$ = 52 eV, transition matrix element effects can be neglected allowing us to determine sublattice symmetry and isospin with high accuracy using a simple theoretical model.

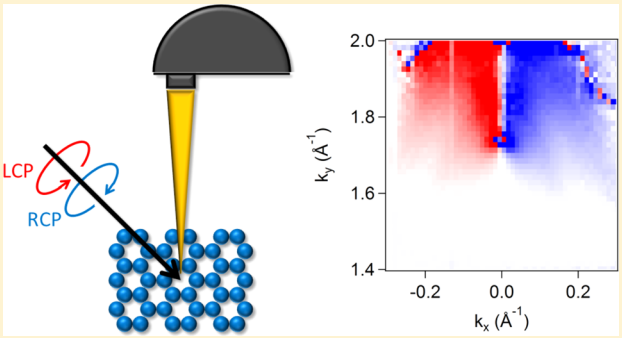

KEYWORDS: *Graphene, sublattice symmetry, isospin, circular dichroism, ARPES*

Graphene, a monolayer of sp^2-hybridized carbon atoms forming a honeycomb lattice, is renowned for its peculiar electronic structure that makes it a promising candidate for possible applications in many different fields, such as graphene-based high-mobility electronic devices,[1] saturable absorbers for the creation of femtosecond laser pulses,[2] sensors for single molecule detection,[3] or even as a building block in anyonic circuits for quantum computation.[4,5] The peculiar electronic structure, where two linearly dispersing bands intersect each other at the Fermi level, can be directly visualized using angle-resolved photoemission spectroscopy (ARPES).[6] There, the interference of photoelectrons emitted by the two carbon atoms within the unit cell leads to the suppression of photocurrent on part of the Fermi surface (dark corridor).[7−11] In principle, the resulting cosine-shaped intensity modulation contains information about the relative phase between the two triangular sublattices (the isospin θ_k) as well as the sublattice symmetry.[9,10] Furthermore, recent polarization-dependent ARPES experiments have revealed that the position of the dark corridor depends on the polarization of the incident photons,[11−13] and that the rotation of the dark corridor with changing light polarization is related to graphene's Berry phase of π.[12,13]

As the electronic properties of graphene crucially depend on both the isospin and the sublattice symmetry (the difference in isospin allows for the crossing of the linearly dispersing bands at the $\bar{K}$-point,[14,15] while the sublattice symmetry is intimately linked to the absence of a band gap at the Dirac point),[6,16,17] it would be desirable to obtain them directly from an ARPES experiment. This information is contained in the photoemission transition matrix elements. Unfortunately, it is masked by an additional intensity modulation caused by the geometry of the experimental setup as well as by final state effects[18] that are often neglected when interpreting ARPES data. Furthermore, it has turned out that the common choice of a single plane wave final state is usually inappropriate.[11] This may explain why the determination of the isospin and the sublattice symmetry in graphene on the basis of multi-Brillouin zone photoemission data resulted in rather large discrepancies from the theoretically predicted values.[10] The alternative approach using Fourier-transformed scanning tunneling microscopy images faces similar difficulties as it is only able to place an upper limit on the degree of sublattice symmetry breaking.[20] A simple solution to this problem would be to find a situation where the influence of spurious effects caused by the experimental geometry and final state wave function on ARPES data is reduced to a minimum.

Here, we show that precise values for isospin and sublattice symmetry can be obtained from ARPES experiments using both right and left circularly polarized light. We will present a simple theoretical model based on refs 7, 9, and 10 that allows us to distinguish the intensity modulation caused by the sublattice interference from the one caused by the setup and by final state effects. We find that for certain photon energies the latter is

Received: February 7, 2012
Revised: July 9, 2012
Published: July 11, 2012

   dx.doi.org/10.1021/nl300512q | *Nano Lett.* 2012, 12, 3900−3904

negligible, which enables us to determine the isospin θ_k and a parameter A that is related to the sublattice symmetry directly from the ARPES data. Furthermore, by exciting the sample with circularly polarized light at different energies, we can rotate the position of the dark corridor in agreement with first-principles calculations.

We prepared graphene monolayers by thermal graphitization of SiC(0001) in ultrahigh vacuum. Details about the sample preparation are given in ref 19. The measurements were done at the Synchrotron Radiation Center (SRC) in Stoughton, Wisconsin at the variable polarization VLS-PGM beamline that delivers right (RCP) and left circular polarization (LCP) of photons in the energy range from 15 to 250 eV. The ARPES setup offers an angular resolution of 0.4° and an energy resolution of better than 10 meV. During measurements the sample was kept at a temperature of 50 K.

Details of our one-step approach to photoemission are given in refs 21−24. The imaginary part of the initial (final) state self-energy is chosen to be 0.05 eV (4 eV). Real parts were incorporated via the energy-independent inner potential. The fully self-consistent electronic structure of free-standing graphene was calculated within the local density approximation to density functional theory using the Kohn−Korringa−Rostoker Green function methodology.[25−27] The absence of the substrate in the calculations is expected to result in deviations from the experimental findings because the SiC substrate induces an n-type doping of the graphene layer and scatters the outgoing photoelectrons which may affect the final state wave function.

In Figure 1a we present measured Fermi surfaces for epitaxial graphene excited with RCP and LCP light of different photon energies, respectively. We find that the position of the dark corridor differs for RCP and LCP light and rotates away from the $\overline{\Gamma K}$ symmetry line. The experimental findings are nicely reproduced by the first-principles calculations displayed in Figure 1b. In order to account for the substrate-induced n-type doping, the calculations in Figure 1b have been shifted to match the experimental Fermi wave vector.

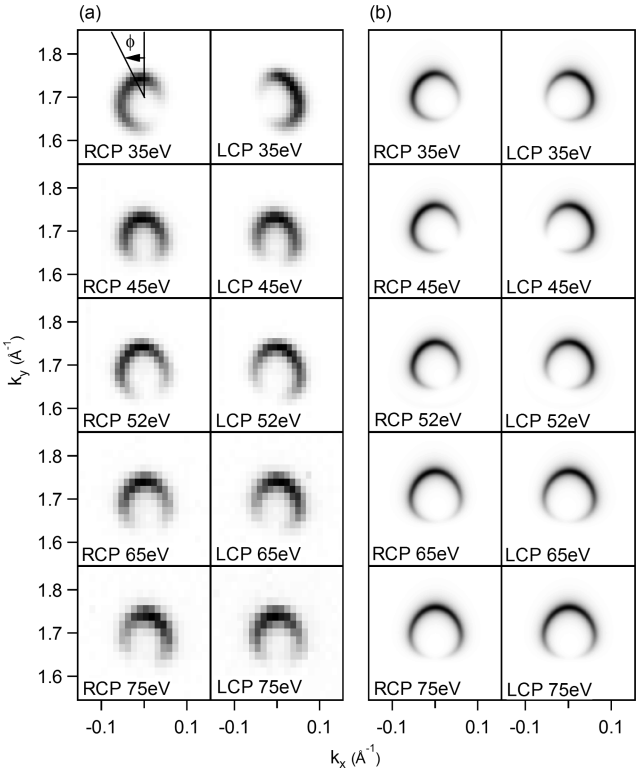

Figure 1. Measured (a) and calculated (b) Fermi surfaces for RCP and LCP light of different energies.

Our density functional theory (DFT) calculations reproduce most of the features of our experimental data. The origin of these features, however, is easier to understand in the framework of a simple phenomenological model based on a tight-binding formalism, which allows us to extract the physical parameters we are interested in by fitting our data. According to Fermi's Golden Rule, the photocurrent I is proportional to the absolute square of the transition matrix element $M = \langle \Psi_f | H | \Psi_i \rangle$, where $\Psi_{i,f}$ are the initial and final state wave functions, respectively, and H is the interaction Hamiltonian. As the graphene lattice has two carbon atoms per unit cell, the π-bands consist of two p_z-orbitals that are either centered on atom A or on atom B. Therefore, we write the initial state wave function as $|\Psi_i\rangle = c_A|p_z, A\rangle \pm c_B|p_z, B\rangle$, where the coefficients c_A and c_B fulfill $|c_A|^2 + |c_B|^2 = 1$ and $c_B/c_A = Ae^{i\theta_k}$[10] with $A = 1$ ($A \neq 1$) for equivalent (inequivalent) sublattices. The + (−) sign corresponds to the conduction (valence) band. Further, we assume that $\langle \Psi_f | H | p_z, B \rangle = e^{-i\phi_0} \langle \Psi_f | H | p_z, A \rangle$. The phase factor $e^{-i\phi_0}$ describes the phase difference between electrons emitted from sublattice A and B, respectively, and has been inserted to account for the experimentally observed rotation of the dark corridor with photon energy. In the following, we will skip the subscript A in $|p_z, A\rangle$ and write $|p_z\rangle$ instead. For our present purpose we do not need to make any assumption about the final state wave function Ψ_f. In this case the photocurrent is given by

$$I \propto |\langle \psi_f | H | \psi_i \rangle|^2 = \left(1 \pm \frac{2A}{1 + A^2} \cos(\theta_k - \phi_0)\right) |\langle \psi_f | H | p_z \rangle|^2$$

The first factor describes the suppression of photoemission intensity inside the dark corridor in agreement with previous models.[9,10] The $(1 \pm \cos \theta_k)$-dependence also follows from ref 7 by expanding the photoemission intensity in the vicinity of the $\overline{K}$-point. The isospin θ_k is expected to vary linearly on a circle around $\overline{K}$.[10] The phase offset ϕ_0 describes the experimentally observed rotation of the dark corridor with photon energy away from $\phi = 180°$ for the conduction band and $\phi = 0°$ for the valence band, where ϕ is defined in the upper left panel of Figure 1a. Apart from this sublattice interference term the intensity is modulated by a second factor $|\langle \Psi_f | H | p_z \rangle|^2$ that depends on the geometry of the experimental setup and on final state effects,[18] that is, it strongly varies with photon energy. If we assume that $I_0 = |\langle \Psi_f | H | p_z \rangle|^2 \approx$ constant within the region of interest around the $\overline{K}$-point (we will show below that this is the case for $h\nu = 52$ eV), the photocurrent can be described by

$$I = I_0 \left(1 \pm \frac{2A}{1 + A^2} \cos(\theta_k - \phi_0)\right) + c \quad (1)$$

where c accounts for the photoemission background. The difference in photocurrent between RCP and LCP light (usually referred to as circular dichroism in the angular distribution (CDAD) of photoelectrons[18]) is best visualized by analyzing the normalized intensity difference $I_{nCDAD} = (I_{RCP} - I_{LCP})/(I_{RCP} + I_{LCP})$. After a careful background subtraction,

dx.doi.org/10.1021/nl300512q | Nano Lett. 2012, 12, 3900−3904

we have $c/I_0 \ll 1$, and we obtain the following expression for the normalized CDAD signal, I_{nCDAD} =

$$\frac{\pm A(\cos(\phi - \phi_{RCP}) - \cos(\phi - \phi_{LCP}))}{1 + A^2 \pm A(\cos(\phi - \phi_{RCP}) + \cos(\phi - \phi_{LCP}))} \quad (2)$$

where $\phi_{RCP,LCP}$ is the position of the dark corridor for RCP and LCP light, respectively.

In Figure 2, we present a quantitative analysis of the data displayed in Figure 1. Figure 2a shows the measured (filled markers) as well as the calculated position (empty markers) of the dark corridor ϕ_0 for RCP (circles) and LCP light (diamonds), respectively, as a function of photon energy. We attribute the observed variation of ϕ_0 with photon energy to a change in the final state. In contrast to the theoretical values which are symmetric with respect to the $\overline{\Gamma K}$ line, the experimental results are symmetric with respect to $\phi_0 \approx -10°$. This discrepancy might be caused by a slight ellipticity of the incident light and/or a small misalignement of the sample.

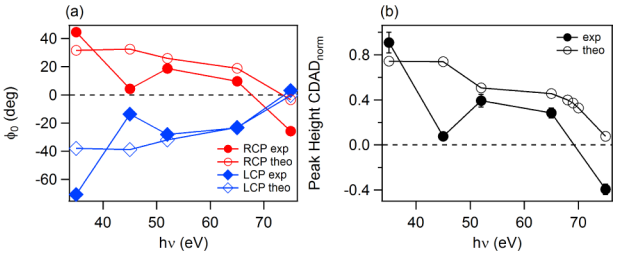

Figure 2. (a) Measured as well as calculated position of the dark corridor ϕ_0 for RCP and LCP light as a function of photon energy; (b) measured as well as calculated peak height of the normalized CDAD signal on the Fermi surface at $E = E_F$ and $k_y = 1.7$ Å^{-1} as a function of photon energy. Negative values are used in case the sign of the CDAD signal is reversed.

In ref 13, the 90° rotation of the dark corridor away from the $\overline{\Gamma K}$ line for a photon energy of 30 eV has been related to the phase angle of the light polarization $\chi = \arctan(A_y/A_x)$, where $A_{x,y}$ is the projection of the incident light field onto the sample surface. Although this purely geometric effect cannot explain the observed photon energy dependence in Figures 1 and 2 (see Supporting Information for details), it correctly reproduces the experimental results for $h\nu$ = 30 eV of ref 13. Furthermore, the claim made in ref 13 that the position of the dark corridor is a direct visual confirmation of the Berry's phase of π seems to be justified only for $h\nu$ = 30 eV, where $\phi_{RCP,LCP} \approx \pm 90°$.

In Figure 2b, we compare the theoretical (filled circles) and the experimental peak height (empty circles) of I_{nCDAD} along a momentum distribution curve at $E = E_F$ and $k_y = 1.7$ Å^{-1} as a function of photon energy. They exhibit the same behavior with a general decrease in band peak height with increasing photon energy. The deviations between experiment and theory around 45 and 75 eV indicate that for these photon energies the theoretical final state wave function differs from the experimental one. This might be related to the absence of the SiC substrate in the calculations.[11] Furthermore, our calculations have shown that for high photon energies ($h\nu$ > 60 eV) the final state wave function changes rapidly. In this case, even a small offset in the theoretical photon energy due to the real part of the self-energy[11] will have a huge effect on the predicted CDAD signal.

Figure 3 compares the energy-integrated normalized CDAD signal of the valence band (note that the position of the dark corridor differs by 180° between the valence band in Figures 3 and 4 and the conduction band in Figures 1 and 2) for two different photon energies $h\nu$ = 52 eV (panel a) and $h\nu$ = 65 eV (panel b), respectively. Red (blue) corresponds to negative (positive) values. The regions around the $\overline{K}$-point where $I_{RCP} = I_{LCP}$ appear white. Prior to energy-integration a Shirley background has been subtracted from the experimental data. In order to access the $\mathbf{k}_\parallel$-dependence of I_{nCDAD}, Figure 3c,d displays line profiles along circles of different radii around the $\overline{K}$-point as indicated in Figure 3a,b. While the normalized CDAD signal at $h\nu$ = 52 eV has one nodal line along the $\overline{\Gamma K}$-direction, two additional nodal lines appear for $h\nu$ = 65 eV. In contrast to the data for $h\nu$ = 65 eV as well as the other photon energies (see Supporting Information), the line profiles for $h\nu$ = 52 eV can be nicely fitted using eq 2 as will be discussed later in the context of Figure 4c. Thus we conclude that for $h\nu$ = 52 eV the assumption that $|\langle\Psi_f|H|p_z\rangle|^2 \approx$ constant within the region of interest around the $\overline{K}$-point holds, which means that the experimental data is mainly determined by the initial state properties we are interested in. We attribute this beneficial situation to a transition in the final state wave function from mostly s- and p-like partial waves for $h\nu$ < 52 eV to mostly d-like partial waves for $h\nu$ > 52 eV that allowed us to homogeneously illuminate the complete Fermi surface of graphene in our previous publication.[11]

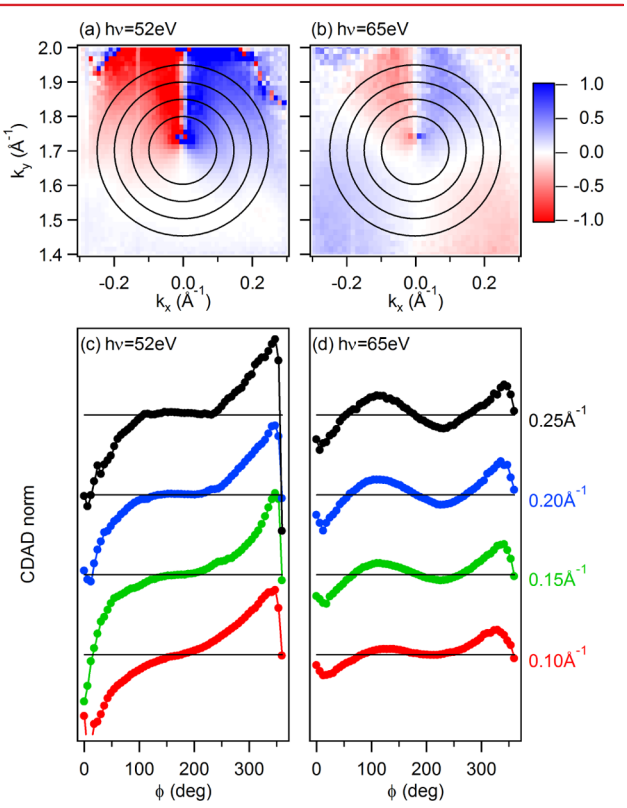

Figure 3. Energy-integrated normalized CDAD signal of the valence band for $h\nu$ = 52 eV (a) and $h\nu$ = 65 eV (b). Red (blue) corresponds to negative (positive) values. Panels (c) and (d) show the variation of I_{nCDAD} on circles with different radii around the $\overline{K}$-point as indicated in panels (a) and (b) for $h\nu$ = 52 eV and $h\nu$ = 65 eV, respectively.

In order to determine the isospin θ_k and the sublattice symmetry parameter A directly from the experimental data,

dx.doi.org/10.1021/nl300512q | Nano Lett. 2012, 12, 3900−3904

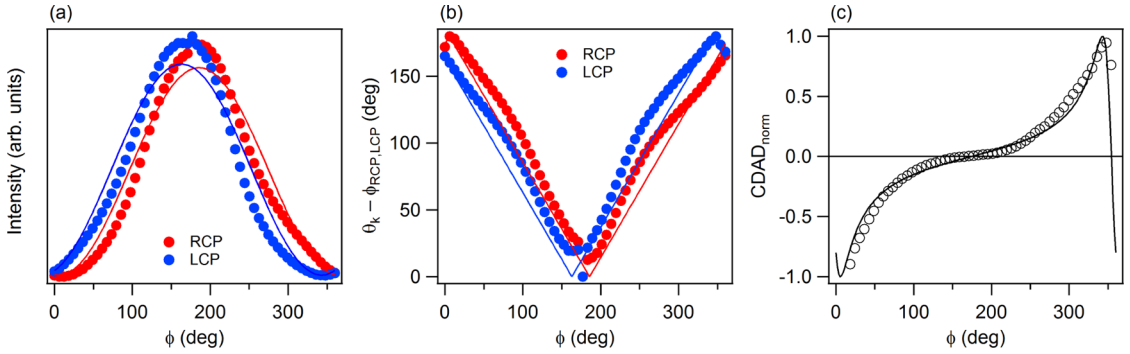

Figure 4. (a) Energy-integrated intensity of the valence band averaged over different radial distances with respect to the $\bar{K}$-point together with a fit based on eq 1. (b) Isospin ($\theta_k - \phi_{RCP,LCP}$) as a function of ϕ. Continuous lines are drawn according to ($\theta_k - \phi_{RCP,LCP}$) = ϕ with $\phi_{RCP} = 6°$ and $\phi_{LCP} = -17°$; (c) normalized CDAD signal on a circle around the $\bar{K}$-point averaged over different radial distances with respect to the $\bar{K}$-point together with a fit based on eq 2.

Figure 4a shows the energy-integrated intensity of the valence band for $h\nu$ = 52 eV averaged over different radial distances from $\bar{K}$. The data points for RCP (LCP) light are shown in red (blue). By fitting this data to the model in eq 1 we can determine the position of the dark corridor for RCP and LCP light, $\phi_{RCP} = (6 \pm 1°)$ and $\phi_{LCP} = (-17 \pm 1°)$. The fits are shown as continuous lines in Figure 4a.

Furthermore, we can directly calculate the ϕ-dependence of the isospin θ_k via $(\theta_k - \phi_{RCP,LCP}) = \arccos((I_1 - I)/I_2)$, where the coefficients I_1 and I_2 are obtained from the maximum and minimum intensity in Figure 4a via $I_1 = (I_{max} + I_{min})/2$ and $I_2 = (I_{max} - I_{min})/2$. The resulting isospin$(\theta_k(\phi) - \phi_{RCP,LCP})$ is shown as dots in Figure 4b. The continuous lines are drawn according to $\theta_k = \phi$ with offsets of $\phi_{RCP} = 6°$ and $\phi_{LCP} = -17°$, respectively. The good agreement gives an experimental confirmation for the assumption that θ_k varies linearly on a circle around the $\bar{K}$-point. The remaining slight deviations from the expected linear behavior might be caused by a non-Shirley background contribution and/or small residual final state effetcs.

In order to also determine the sublattice symmetry parameter A we have to make use of the normalized CDAD signal in eq 2 that neither depends on the intensity I_0 which drops out because of the normalization, nor on the background c as $c/I_0 \ll 1$ after subtracting a Shirley background. In Figure 4c, we averaged the normalized CDAD data from Figure 3a,c over different radial distances from the $\bar{K}$-point. The resulting data points (open black spheres) can be nicely fitted to the model in eq 2 with $A = 1.0 \pm 0.1$ (see continuous line in Figure 4c). In principle this result can be directly deduced from the amplitude of I_{nCDAD} in Figures 3c and 4c as this amplitude can only be smaller than one if $A \neq 1$, if $c/I_0 \ll 1$ is not fulfilled (which we exclude by subtracting a Shirley background), or if $|\langle \Psi_f | H | p_z \rangle|^2 \approx$ constant is not fulfilled (which we exclude by our careful choice of the photon energy). Thus, we are able to determine the parameters c_A and c_B in the initial state wave function of graphene as $|c_{A,B}|^2 = (0.50 \pm 0.05)$ and $c_B = (1.0 \pm 0.1)c_A e^{i\phi}$.

In summary, we have developed a simple phenomenological model where the photocurrent in graphene is proportional to the product of the well-known sublattice interference term and an additional term that depends on the geometry of the experimental setup as well as on the final state wave function. By considering the normalized CDAD signal we were able to identify $h\nu$ = 52 eV as a photon energy where the latter contribution is negligible so that the experimental data is mainly determined by the properties of the initial state. We confirmed experimentally that the isospin θ_k varies linearly on a circle around $\bar{K}$ and that the value of the sublattice symmetry parameter is $A = 1.0 \pm 0.1$ obtaining a much better agreement with theoretical predictions than previous results.[10,20] Therefore, our results confirm that the sublattice symmetry in epitaxial graphene is conserved which makes a substrate-induced band gap opening unlikely.

■ ASSOCIATED CONTENT

Supporting Information

The Supporting Information contains experimental results for photon energies that are not shown in the main paper, as well as a more detailed comparison with with ref 13. This material is available free of charge via the Internet at http://pubs.acs.org.

■ AUTHOR INFORMATION

Corresponding Author

*E-mail: isabella.gierz@mpsd.cfel.de;.

Present Address

[⊥]Max-Planck Research Group for Structural Dynamics, University of Hamburg, Center for Free Electron Laser Science, 22607 Hamburg, Germany.

Notes

The authors declare no competing financial interest.

■ ACKNOWLEDGMENTS

The authors thank U. Starke, C. Riedl, C. L. Frewin, C. Locke, and S. E. Saddow for hydrogen etching of the SiC substrates and J. Henk for many stimulating discussions. C.R.A. acknowledges funding by the Emmy-Noether-Program of the Deutsche Forschungsgemeinschaft. This work is based upon research conducted at the Synchrotron Radiation Center of the University of Wisconsin-Madison that is funded by the National Science Foundation under Award No DMR-0537588.

■ REFERENCES

(1) Novoselov, K. S.; Geim, A. K.; Morozov, S. V.; Jiang, D.; Zhang, Y.; Dubonos, S. V.; Grigorieva, I. V.; Firsov, A. A. *Science* **2008**, *306*, 666−669.

(2) Bonaccorso, F.; Sun, Z.; Hasan, T.; Ferrari, A. C. *Nat. Photonics* **2010**, *4*, 611−622.

(3) Schedin, F.; Geim, A. K.; Morozov, S. V.; Hill, E. W.; Blake, P.; Katsnelson, M. I.; Novoselov, K. S. *Nat. Mater.* **2007**, *6*, 652−655.

(4) Bolotin, K. I.; Ghahari, F.; Shulman, M. D.; Stormer, H. L.; Kim, P. *Nature* **2009**, *462*, 196−199.

(5) Du, X.; Skachko, I.; Duerr, F.; Luican, A.; Andrei, E. Y. *Nature* **2009**, *462*, 192−195.
(6) Bostwick, A.; Ohta, T.; Seyller, T.; Horn, K.; Rotenberg, E. *Nat. Phys.* **2007**, *3*, 36−40.
(7) Shirley, E. L.; Terminello, L. J.; Santoni, A.; Himpsel, F. J. *Phys. Rev. B* **1995**, *51*, 13614−13622.
(8) Kuemmeth, F.; Rashba, E. I. *Phys. Rev. B* **2009**, *80*, 241409(R).
(9) Mucha-Kruczyński, M.; Tsyplyatyev, O.; Grishin, A.; McCann, E.; Falko, V. I.; Bostwick, A.; Rotenberg, E. *Phys. Rev. B* **2008**, *77*, 195403.
(10) Jung, W. S.; Leem, C. S.; Kim, C.; Park, S. R.; Park, S. Y.; Kim, B. J.; Rotenberg, E.; Kim, C. *Phys. Rev. B* **2010**, *82*, 235105.
(11) Gierz, I.; Henk, J.; Höchst, H.; Ast, C. R.; Kern, K. *Phys. Rev. B* **2011**, *83*, 121408(R).
(12) Hwang, C.; Park, C.-H.; Siegel, D. A.; Fedorov, A. V.; Louie, S. G.; Lanzara, A. *Phys. Rev. B* **2011**, *84*, 125422.
(13) Liu, Y.; Bian, G.; Miller, T.; Chiang, T.-C. *Phys. Rev. Lett.* **2011**, *107*, 166803.
(14) Wallace, P. R. *Phys. Rev.* **1947**, *71*, 622−634.
(15) Slonczewski, J. C.; Weiss, P. R. *Phys. Rev.* **1958**, *109*, 272−279.
(16) Zhou, S. Y.; Gweon, G.-H.; Fedorov, A. V.; First, P. N.; de Heer, W. A.; Lee, W.-H.; Guinea, F.; Castro Neto, A. H.; Lanzara, A. *Nat. Mater.* **2007**, *6*, 770−775.
(17) Rotenberg, E.; Bostwick, A.; Ohta, T.; McChesney, J. L.; Seyller, T.; Horn, K. *Nat. Mater.* **2007**, *7*, 258−259.
(18) Schönhense, G. *Phys. Scr.* **1990**, *T31*, 255−275.
(19) Gierz, I.; Suzuki, T.; Weitz, R. T.; Lee, D. S.; Krauss, B.; Riedl, C.; Starke, U.; Höchst, H.; Smet, J. H.; Ast, C. R.; Kern, K. *Phys. Rev. B* **2010**, *81*, 235408.
(20) Brihuega, I.; Mallet, P.; Bena, C.; Bose, S.; Michaelis, C.; Vitali, L.; Varchon, F.; Magaud, L.; Kern, K.; Veuillen, J. Y. *Phys. Rev. Lett.* **2008**, *101*, 206802.
(21) Arpiainen, V.; Zalobotnyy, V.; Kordyuk, A. A.; Borisenko, S. V.; Lindroos, M. *Phys. Rev. B* **2008**, *77*, 024520.
(22) Pendry, J. B. *Surf. Sci.* **1976**, *57*, 679−705.
(23) Hopkinson, J. F. L.; Pendry, J. B.; Titterington, D. J. *Comput. Phys. Commun.* **1981**, *19*, 69.
(24) Lindroos, M.; Sahrakorpi, S.; Bansil, A. *Phys. Rev. B* **2002**, *65*, 054514.
(25) Bansil, A.; Kaprzyk, S. *Phys. Rev. B* **1991**, *43*, 10335−10339.
(26) Kaprzyk, S.; Bansil, A. *Phys. Rev. B* **1990**, *42*, 7358−7362.
(27) Bansil, A.; Kaprzyk, S.; Mijnarends, P. E.; Tobola, J. *Phys. Rev. B* **1999**, *60*, 13396−13412.